On neural recording using nanoprotrusion electrodes

Liang Guo[1,2]

[1] Department of Electrical and Computer Engineering, The Ohio State University, Columbus, OH, United States of America
[2] Department of Neuroscience, The Ohio State University, Columbus, OH, United States of America

E-mail: guo.725@osu.edu

Received xxxxxx
Accepted for publication xxxxxx
Published xxxxxx

Abstract

Objective. Nano neuroelectrodes, often adopting a nanoprotrusion structure, are promising for improved chronic reliability and capability of both extracellular and intracellular recordings. However, a complete theoretical foundation has yet to be established, significantly impeding further developments and applications. This paper derives analytical solutions to this extracellular and intracellular recording problem of nanoprotrusion electrodes, unraveling the underlying recording mechanisms and elucidating the natures of different recordings. *Approach.* Advanced circuit modeling and analysis techniques from the electrical engineering discipline are introduced to this cutting-edge, interdisciplinary problem, and an analytical framework is developed to produce closed-form solutions that offer clear images on the recording mechanisms, nature of signals, and interplays between key interface parameters. *Main results.* The results show that the "intracellular-like" recording after membrane poration contains fractions of both intracellular action potential (iAP) and extracellular field potential (eFP). When recording using multiple nanoprotrusion electrodes on the same conductive substrate, while the signal itself is only slightly enhanced, the recording is substantially enhanced, comparing to using a single electrode. Having the substrate unpassivated can distort the iAP component more with the eFP component, and the portion uncovered by cell can further severely compromise the recording quality. *Significance.* Through key conceptual breakthroughs, this present work advanced our prior knowledge on this topic to a critical level capable of deriving closed-form analytical solutions. These findings are significant to advance the theory and practice of nano neuroelectrode technologies.

Keywords: nanopillar electrodes, tight seal, membrane poration, intracellular-like action potential, recording mechanism, equivalent electrical circuit model

1. Introduction

Developing nano-electrophysiological technologies capable of mapping functional connectivity of neuronal circuits, probing their information processing patterns, and studying their physiological or pathological functions is of great importance to the neuroscience and neuroengineering communities. For neuroscience, as well as the pharmaceutical industry, technologies enabling long-term, simultaneous multisite, intracellular recording and stimulation from many neurons under *in vitro* and *in vivo* conditions are highly demanded in place of the short-term, low-throughput conventional technologies such as patch-clamp recording or the less sensitive planar multielectrode array technology [1].

The deciphered neurobiological mechanisms can promote biologically inspired artificial intelligence designs for better performance, and may even stimulate electronic-biological hybrid computing systems that supersede the performance of either implementation alone.

Although a few intracellular recording examples using planar multielectrode arrays through electro- or optoporation exist [2, 3], the large area of membrane poration (and thus leakage) nonetheless could cause considerable damage to the cell and consequently shorten the meanful observation window. Excitingly, nanoelectrode-enhanced implantable neural probes that can form long-term stable, intimate interfaces with target neurons and record or stimulate intracellularly can open up new possibilities for large-scale studies of neuronal circuit dynamics *in vivo* and advanced neural prosthetics [4-7]. These exciting applications can be envisioned to become available within a number of years, in witness of recent fast advances in this class of nano-electrophysiological technologies [4, 5, 8-12]. The most straightforward design of this class of nanoelectrodes assumes a nanoprotrusion structure [4, 8, 11, 12] that can form an intimate contact to the cell membrane (Figure 1). Actually, it is such an intimate contact that brings this type of nanoelectrodes with many distinctive advantages in neuronal recording, namely enhanced recording quality in terms of signal-to-noise ratio (SNR), long-term interface stability, and smooth switching between extracellular and intracellular recording modes. Their other technical advantages also include scalability, compatibility and integrability with complementary metal-oxide–semiconductor (COMS) circuitry to allow on-chip signal multiplexing and processing [8].

However, further advance and application of this class of nanoelectrode technologies are presently impeded by poor understandings on the recording mechanisms and recorded signals. On the one hand, this class of nanotechnologies has only emerged for a decade [1], many earlier established theoretical work cannot cover the unique new experimental configurations [13-15]. On the other hand, although a few insightful models and simulations have been produced by relevant leading scientists with different levels of details [1, 8, 12, 16, 17], these existing models can neither produce simulation results to accurately capture the dynamics of empirical recordings nor explain the deviations. Consequently, a clear and complete mechanistic theory that can fully account for the empirical results has yet to be established.

To address this critical knowledge gap, I introduced advanced circuit modeling and analysis techniques from the electrical engineering discipline to this cutting-edge, interdisciplinary problem and developed an analytical framework to produce closed-form solutions that offer clear insights on the recording mechanisms, nature of signals, and

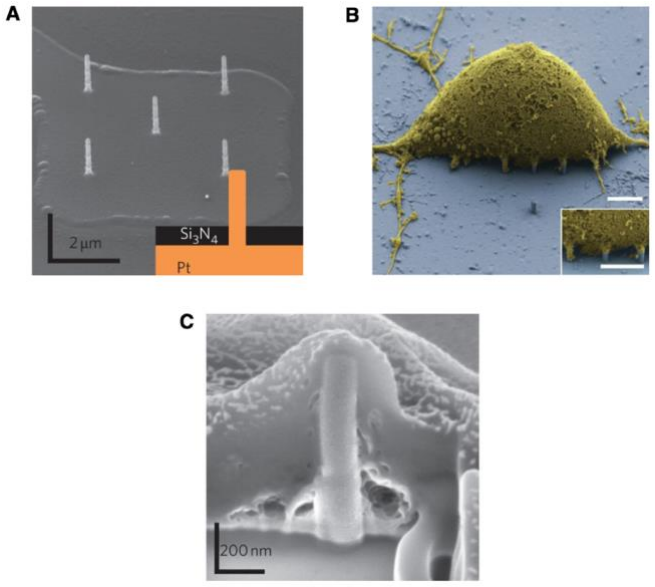

Figure 1. Typical nanoprotrusion electrodes and cell interface. (**A**), SEM image of an array of five nanoprotrusion electrodes fabricated on a passivated planar microelectrode. The contour of the square microelectrode is visible. (**B**), SEM image of a rat cortical cell (3 DIV, false-colored yellow) on top of an array of nanoprotrusion electrodes (false-colored blue; scale bar, 2.5 µm), showing nanoprotrusions interfacing with the cellular membrane (inset; scale bar, 2.5 µm). (**C**), SEM image of the cell–nanoprotrusion electrode interface shows that the electrode is fully engulfed by the cell. Figure reproduced with permission from: (**A**), (**C**), Ref. [4], © 2012 NPG; (**B**), Ref. [8], © 2012 NPG.

interplays between key interface parameters. Through key conceptual breakthroughs (see *Methods*), this present work advanced our prior knowledge on this topic [1, 12, 15, 16] to a critical level capable of deriving closed-form analytical solutions.

While intracellular recordings can obtain a unique waveform of the action potential (AP), extracellular recordings are complicated by the location, size, and shape of the electrode, as well as neighboring neural structures [13, 14, 18]. Fortunately, the recording environment of nanoprotrusion electrodes is a very special situation well isolated from interferences in the surrounding macro cell-electrolyte environment (Figure 1B and 1C), and the size and shape of these electrodes are relatively consistent [4, 8, 11, 12]. Furthermore, as it takes less than 1/1000 of its duration for the AP to pass over the nanojunctional membrane area, we can assume the micro membrane surrounding the nanoprotrusion electrode to be excited in synchrony and thus can ignore the propagation effect of the AP on the recording. These conditions make it possible to derive a unique solution to this particular recording situation.

2. Methods

2.1 Key conceptual developments

The following two key conceptual developments advanced the equivalent electrical circuit model of a neuron to a critical level capable of deriving a closed-form analytical relationship

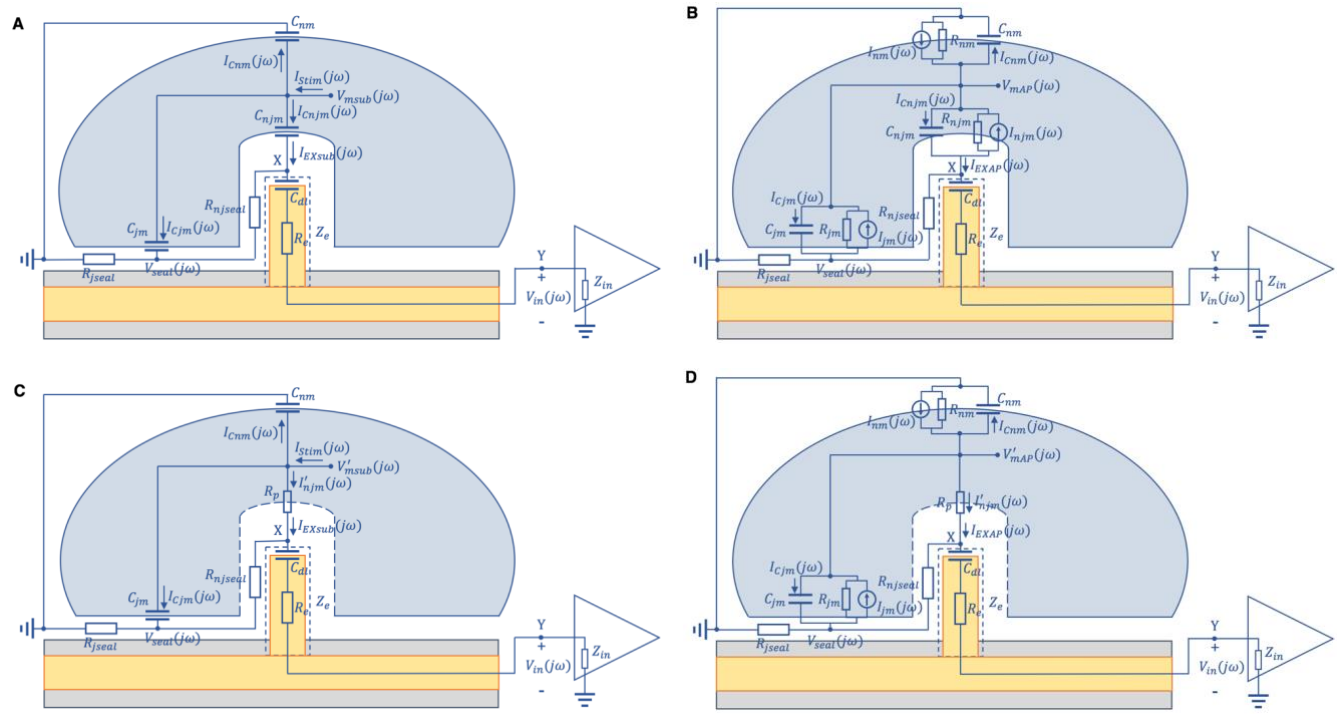

Figure 2. Abstracted models of the nanoprotrusion electrode-cell membrane interfaces and their equivalent electrical circuits. (**A**) and (**B**), Equivalent electrical circuits for extracellular recording during subthreshold depolarization and AP, respectively. (**C**) and (**D**), Equivalent electrical circuits for intracellular-like recording after membrane poration during subthreshold depolarization and AP, respectively. Subscripts: *nm*, nonjunctional membrane; *jm*, junctional membrane; *njm*, nanojuctional membrane; *jseal*, junctional seal; *njseal*, nanojunctional seal; *Stim*, stimulation; *EX*, extracellular; *sub*, subthreshold depolarization phase; *AP*, action potential phase; *dl*, electric double layer; *p*, porated. *X* is the extracellular point where the potential is investigated. In (**B**) and (**D**), the opened ion channel resistances R_{nm}, R_{jm} and R_{njm} are treated as the internal resistances of the respective transmembrane current sources, and $I_{Cnm}(j\omega)$, $I_{Cjm}(j\omega)$, and $I_{Cnjm}(j\omega)$ are virtual capacitive transmembrane currents.

between the transmembrane potential $V_m(j\omega)$ and extracellular potential $V_X(j\omega)$ during subthreshold depolarization and suprathreshold action potential (AP), respectively.

2.1.1 Omission of passive membrane resistance R_m during subthreshold depolarization in the model.

During subthreshold depolarization, the leaking current through the passive membrane resistance R_m is ignored, as R_m is very high, *e.g.* 150 ~ 600 MΩ for HEK293 cells [8]. Given values of the membrane resistance and capacitance, the majority of passive membrane current flows through C_m at ~1 kHz in the parallel circuit, according to $\left|\frac{I_{C_m}}{I_{R_m}}\right| = \omega R_m C_m = \omega\tau$. This justification makes the outward extracellular current $I_{Esub}(j\omega) = I_{Stim}(j\omega) \approx I_{Cmsub}(j\omega)$ a reasonable approximation.

2.1.2 Virtual capacitive transmembrane current during AP.

For an imaginary neuron suspended in an electrolyte, during the AP, there is a membrane capacitive current $I_{CmAP}(j\omega) \approx -I_{AP}(j\omega)$ to close the circuit. As the neuron has uniform current densities (current per unit membrane area) across its entire membrane surface, this capacitive current balances the inward Na^+ current during the depolarization phase and the outward K^+ current during repolarization. A close scrutinization of this capacitive current from the biophysical aspect of membrane depolarization and repolarization makes us aware that it is different in nature from the capacitive current $I_{Cmsub}(j\omega) \approx I_{Stim}(j\omega)$ during the subthreshold depolarization, which crosses the membrane and flows into the extracellular space. In contrast, $I_{CmAP}(j\omega)$ does not flows into the extracellular space. Its existence is merely a passive consequence of the discharging or recharging of the transmembrane voltage $V_{mAP}(j\omega)$ by the $I_{Na}(j\omega)$ or $I_K(j\omega)$ according to $I_C(j\omega) = C_m \cdot j\omega V_{mAP}(j\omega)$. Take the discharging phase by $I_{Na}(j\omega)$ as an example. At rest, the membrane is negatively charged inside with anions accumulated on the inner membrane surface and cations on the outer membrane surface. When the subthreshold depolarization reaches the AP threshold, noticeable Na^+ ions start to flow across the membrane from the outside. The transportation of one Na^+ ion from the outside to the inside, where it "neutralizes" an anion, depolarizes (reduces) the $V_{mAP}(j\omega)$, which requires removal of one charge from both sides (a positive charge from the outside and a negative charge from the inside) of the membrane capacitor C_m according to $Q = C_m V_{mAP}(j\omega)$. Interestingly, this physical process automatically meets this requirement of charge pair removal without an actual capacitive current flowing to either the

Table 1. Analytical solutions for different recording configurations.

single nanoprotrusion electrode			
	subthreshold potential	**AP**	**recorded potential**
extracellular recording	$v_X(t) \approx [\beta_{njm}R_{njseal} + (\beta_{jm}+\beta_{njm})R_{jseal}]C_m \cdot \frac{dv_m(t)}{dt}$ (1)	$v_X(t) = -[\beta_{njm}R_{njseal} + (\beta_{jm}+\beta_{njm})R_{jseal}]C_m \cdot \frac{dv_m(t)}{dt}$ (2)	$V'_X(j\omega) = \frac{1}{1+\frac{R'_s}{Z_e+Z_{in}}}V_X(j\omega)$ (5)
intracellular recording after membrane poration	$v_X(t) = \frac{R_{jseal}+R_{njseal}}{R_{jseal}+R_p+R_{njseal}}v'_m(t)$ (3)	$v_X(t) \approx \frac{R_{njseal}}{R_p+R_{njseal}}v'_m(t) - \frac{R_pR_{jseal}}{R_p+R_{njseal}}C_{jm} \cdot \frac{dv'_m(t)}{dt}$ (4)	$V_{in}(j\omega) = \frac{Z_{in}}{Z''_e+Z_{in}}V_X(j\omega)$ (6)
multiple nanoprotrusion electrodes			
	subthreshold potential	**AP**	**recorded potential**
extracellular recording	$v_X(t) \approx [\beta_{njm}R_{njseal} + (\beta_{jm}+n\beta_{njm})R_{jseal}]C_m \cdot \frac{dv_m(t)}{dt}$ $\approx [\beta_{njm}R_{njseal} + (\beta_{jm}+\beta_{njm})R_{jseal}]C_m \cdot \frac{dv_m(t)}{dt}$ (7)	$v_X(t) = -[\beta_{njm}R_{njseal} + (\beta_{jm}+n\beta_{njm})R_{jseal}]C_m \cdot \frac{dv_m(t)}{dt}$ $\approx -[\beta_{njm}R_{njseal} + (\beta_{jm}+\beta_{njm})R_{jseal}]C_m \cdot \frac{dv_m(t)}{dt}$ (8)	$V'_X(j\omega) = \frac{1}{1+\frac{R''_s}{\frac{Z_e}{n}+Z_{in}}}V_X(j\omega)$ (11)
intracellular recording after membrane poration	$v_X(t) = \frac{nR_{jseal}+R_{njseal}}{nR_{jseal}+R_p+R_{njseal}}v'_m(t)$ $\approx \frac{R_{jseal}+R_{njseal}}{R_{jseal}+R_p+R_{njseal}}v'_m(t)$ (9)	$v_X(t) \approx \frac{R_{njseal}}{R_p+R_{njseal}}v'_m(t) - \frac{R_pR_{jseal}}{R_p+R_{njseal}}C_{jm} \cdot \frac{dv'_m(t)}{dt}$ (10)	$V_{in}(j\omega) = \frac{Z_{in}}{\tilde{Z}''_e+Z_{in}}V_X(j\omega)$ (12)

$R'_s = R_{njseal} + R_{jseal}$. $Z''_e = Z_e + R'_s$ is the *in-situ* electrode impedance of the nanoprotrusion electrode measured with the electrolyte at the exterior of the nonjunctional membrane grounded, to differentiate it from the conventional Z'_e measured without the tight membrane seals. $R''_s = \frac{R_{njseal}}{n} + R_{jseal}$, and $\tilde{Z}''_e = \frac{Z_e}{n} + R''_s$.

extracellular or intracellular space. This conclusion can be similarly extended to the recharging phase where the K_+ current takes effect. Thus, this type of transmembrane capacitive current $I_{CmAP}(j\omega)$ is termed as a "virtual" current. This justification makes the outward extracellular current $I_{EAP}(j\omega) = -I_{AP}(j\omega) = -(I_{Na}(j\omega) - I_K(j\omega))$ for neurons a reasonable representation.

2.2 Extracellular recording by a single nanoprotrusion electrode

2.2.1 Subthreshold depolarization phase. During subthreshold depolarization (Figure 2A), the overall equivalent outward transmembrane current $I_{Esub}(j\omega) = I_{Stim}(j\omega) \approx I_{Cmsub}(j\omega)$ is now split into three portions corresponding to those of the cell membrane. Assuming that the nanoprotrusion doesn't distort capacitive properties of the membrane and that the membrane is spatially uniform (*i.e.*, maintaining a uniform specific capacitance), we define $C_{nm}: C_{jm}: C_{njm}: C_m = \beta_{nm}: \beta_{jm}: \beta_{njm}: 1$. The transmembrane current $I_{Cnjm}(j\omega)$ is minimally affected by the nanojunctional seal (modeled electrically by R_{njseal}, see *Supplementary Methods* for justification), so that the entire cell membrane can be considered to have a uniform transmembrane current density and $I_{Cnjm}(j\omega) = \beta_{njm}I_{Cmsub}(j\omega)$ can be approximated as $\beta_{njm}I_{Stim}(j\omega)$. And the portion of $I_{Esub}(j\omega)$ exiting the nanojunctional membrane is $I_{EXsub}(j\omega) = \beta_{njm}I_{Stim}(j\omega) \approx I_{Cnjm}(j\omega)$. Thus, we have

$$\begin{aligned} V_{Xsub}(j\omega) &= R_{njseal}I_{Cnjm}(j\omega) + R_{jseal}(I_{Cjm}(j\omega) + I_{Cnjm}(j\omega)) \\ &\approx [\beta_{njm}R_{njseal} + (\beta_{jm}+\beta_{njm})R_{jseal}]I_{Stim}(j\omega) \\ &= [\beta_{njm}R_{njseal} + (\beta_{jm}+\beta_{njm})R_{jseal}]C_m \cdot j\omega V_{msub}(j\omega) \end{aligned} \quad \text{(M1)}$$

The time-domain version of equation (M1) corresponds to equation (1) in Table 1. Therefore, $V_{Xsub}(j\omega)$ is proportional to the first time derivative of $V_{msub}(j\omega)$.

2.2.2 AP phase. The equivalent electrical circuit during AP is shown in Figure 2B. Assuming that the nanoprotrusion doesn't distort the distributions of transmembrane ion channels, as the cell membrane functions similarly to a self-propelled battery, the transmembrane current density in the nanojunctional membrane is not affected by the nanojunctional seal R_{njseal} (see *Supplementary Methods* for justification), and we have $I_{njm}(j\omega) = \beta_{njm}I_{AP}(j\omega)$, where $I_{AP}(j\omega) = I_{Na}(j\omega) - I_K(j\omega) = I_{nm}(j\omega) + I_{jm}(j\omega) + I_{njm}(j\omega)$ is the overall transmembrane AP current. The equivalent outward transmembrane current passing Point X is $I_{EXAP}(j\omega) = -I_{njm}(j\omega)$. Note that $I_{Cjm}(j\omega)$ and $I_{Cnjm}(j\omega)$ are virtual capacitive currents. Following a similar analysis, we have

$$V_{XAP}(j\omega) = -[\beta_{njm}R_{njseal} + (\beta_{jm}+\beta_{njm})R_{jseal}]C_m \cdot j\omega V_{mAP}(j\omega) \quad \text{(M2)}$$

The time-domain version of equation (M2) corresponds to equation (2) in Table 1. Thus, $V_{XAP}(j\omega)$ is proportional to the *negative* first time derivative of the intracellular action potential (iAP) $V_{mAP}(j\omega)$.

2.3 Recording by a single nanoprotrusion electrode after membrane poration

Next, let's consider the recording of an "intracellular-like" AP by the nanoprotrusion electrode after electro- or opto-poration of the nanojunctional membrane [4, 8, 11, 12].

Electrically, the cytosol is now connected to the electrolyte in the nanojunction through the nanopores, which are modeled as a lumped resistor R_p as illustrated in Figure 2C and 2D. To the whole cell, the value of R_p (~2 GΩ) is significant due to its nanoscale cross-sectional area [8]. These nanopores thus provide a resistive leaking path to the intracellular currents, which slightly diminishes the iAP $V_m(j\omega)$ in the intact cell to $V'_m(j\omega)$.

2.3.1 Subthreshold depolarization phase. During subthreshold depolarization (Figure 2C), the equivalent outward transmembrane current $I_{Esub}(j\omega) = I_{Stim}(j\omega)$ is still split into three parts corresponding to three parts of the cell membrane: $I_{Cnm}(j\omega)$ and $I_{Cjm}(j\omega)$ as before, and a resistive current $I'_{njm}(j\omega)$ through R_p. Solving this circuit (see *Supplementary Methods*) gives an analytical solution:

$$V_{Xsub}(j\omega) = V'_{msub}(j\omega) - \frac{\frac{R_p}{R_{jseal}+R_p+R_{njseal}}}{j\omega\frac{C_{jm}R_{jseal}(R_p+R_{njseal})}{R_{jseal}+R_p+R_{njseal}}+1} V'_{msub}(j\omega) \quad \text{(M3)}$$

The second term corresponds to the voltage drop across R_p. The modulating factor is a first-order lowpass filter with a passband gain $G = \frac{R_p}{R_{jseal}+R_p+R_{njseal}}$ (*e.g.*, 0.7) and a -3-dB cutoff frequency $f_c = \frac{R_{jseal}+R_p+R_{njseal}}{2\pi C_{jm}R_{jseal}(R_p+R_{njseal})} \approx \frac{1}{2\pi C_{jm}R_{jseal}}$ (*e.g.*, 76 kHz) [19]. Because the frequency spectrum (< 1 kHz) of $V'_{msub}(j\omega)$ falls within its passband, this filter simply reduces to a scaling factor of G. Thus, equation (M3) becomes

$$V_{Xsub}(j\omega) = \frac{R_{jseal}+R_{njseal}}{R_{jseal}+R_p+R_{njseal}} V'_{msub}(j\omega) \quad \text{(M4)}$$

The time-domain version of equation (M4) corresponds to equation (3) in Table 1. This equation is simply a voltage-divider circuit, **indicating that no current is flowing across C_{jm} (i.e., $I_{Cjm}(j\omega) = 0$)**.

2.3.2 AP phase. During AP (Figure 2D), the nonjunctional and junctional membranes generate the AP current $I'_{AP}(j\omega) = I_{nm}(j\omega) + I_{jm}(j\omega)$, which generates the iAP $V'_{mAP}(j\omega)$ by charging the $C_{nm} + C_{jm}$ after deducting the leakage $I'_{njm}(j\omega)$ through R_p. It is noted that $V'_{mAP}(j\omega)$ is slightly lower than $V_{mAP}(j\omega)$ when the nanojunctional membrane is intact, as the total current charging $C_{nm} + C_{jm}$ is smaller than $I'_{AP}(j\omega)$ due to the leakage, though the leaking current $I'_{njm}(j\omega)$ is minute and minimally affects the $V_{mAP}(j\omega)$. Solving this circuit (see *Supplementary Methods*) gives

$$V_{XAP}(j\omega) \approx \frac{R_{njseal}}{R_p+R_{njseal}} V'_{mAP}(j\omega) - \frac{R_pR_{jseal}}{R_p+R_{njseal}} C_{jm} \cdot j\omega V'_{mAP}(j\omega) \quad \text{(M5)}$$

The time-domain version of equation (M5) corresponds to equation (4) in Table 1. Thus, the extracellular potential $V_{XAP}(j\omega)$ has two components with a component directly proportional to the iAP itself due to the leaking nanojunctional membrane minus a scaled first time derivative of the iAP due to the junctional membrane current. The second term is actually a scaled version of the extracellular field potential at the junctional cleft. Therefore, the $V_{XAP}(j\omega)$ at Point X during membrane poration comprises fractions of both the iAP and extracellular field potential (eFP). As the amplitude of the first term is substantially (two orders of magnitude) larger than that of the second, the overall $V_{XAP}(j\omega)$ looks like a scaled version of the iAP [4, 8, 11, 12].

The recorded signal $V_{in}(j\omega)$ is determined by equation (6) in Table 1, further incorporating both an amplitude attenuation and a high-pass filtering. Table 2 shows the estimated amplitudes of $v_{XAP}(t)$ using parameters from literature. The difference in the amplitudes of $v_{XAP}(t)$ before and after nanojunctional membrane poration (equation (M2) vs. (M5)) is a direct result of the difference between the nanojunctional membrane current $I_{njm}(j\omega)$ (in pA) and the leaking current $I'_{njm}(j\omega)$ (in nA), which reflects a substantially enhanced recording after membrane poration [4, 8, 12].

2.4 Recording by multiple nanoprotrusion electrodes on the same planar microelectrode

The equivalent electrical circuits with n nanoprotrusion electrodes are shown in Figure 3. If the surface of the planar microelectrode is passivated [4, 8], these circuits are the same as the those with only one nanoprotrusion electrode in Figure 2, except for a scaling factor n to the parameters in the nanojunction (see *Supplementary Methods* for derivation).

2.4.1 Extracellular recording. For extracellular recording (Figure 3A and 3B), with parameter substitutions in equation (M1) and (M2), we have

$$\begin{aligned} V_{Xsub}(j\omega) &\approx \left[\beta_{njm}R_{njseal} + (\beta_{jm} + n\beta_{njm})R_{jseal}\right]C_m \cdot j\omega V_{msub}(j\omega) \\ &\approx \left[\beta_{njm}R_{njseal} + (\beta_{jm} + \beta_{njm})R_{jseal}\right]C_m \cdot j\omega V_{msub}(j\omega) \end{aligned} \quad \text{(M6)}$$

$$\begin{aligned} V_{XAP}(j\omega) &= -\left[\beta_{njm}R_{njseal} + (\beta_{jm} + n\beta_{njm})R_{jseal}\right]C_m \cdot j\omega V_{mAP}(j\omega) \\ &\approx -\left[\beta_{njm}R_{njseal} + (\beta_{jm} + \beta_{njm})R_{jseal}\right]C_m \cdot j\omega V_{mAP}(j\omega) \end{aligned} \quad \text{(M7)}$$

The time-domain versions of equation (M6) and (M7) correspond to equation (7) and (8) in Table 1.

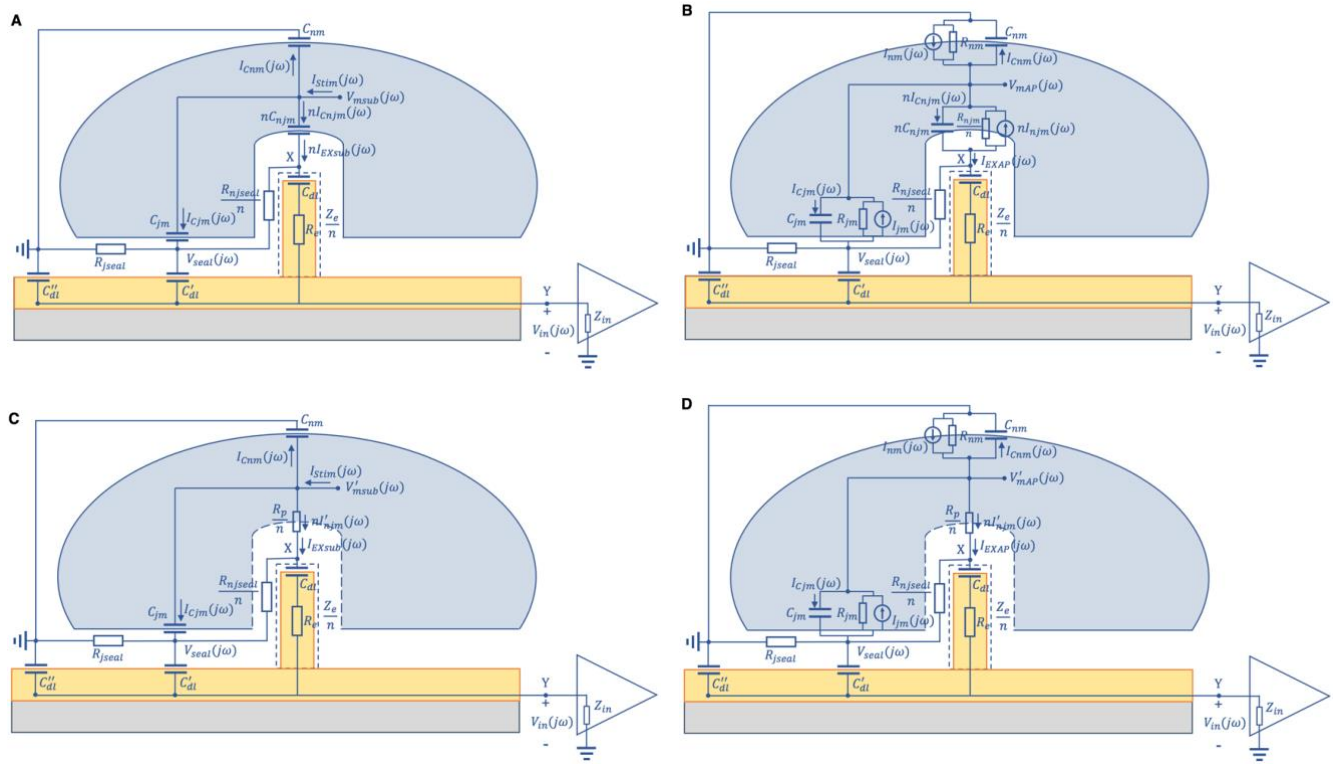

Figure 3. Abstracted models of multiple nanoprotrusion electrode-cell membrane interfaces. (**A**) and (**B**), Equivalent electrical circuits for extracellular recording during subthreshold depolarization and AP, respectively. (**C**) and (**D**), Equivalent electrical circuits for intracellular-like recording after membrane poration during subthreshold depolarization and AP, respectively. Note that the *n* nanoprotrusion electrodes are illustrated as an equivalent nanoprotrusion electrode with proper parameter adjustments. See Figure S5 for derivation.

Recording after membrane poration. After membrane poration (Figure 3C and 3D), with parameter substitutions in equation (M4) and (M5), we have

$$V_{Xsub}(j\omega) = \frac{nR_{jseal}+R_{njseal}}{nR_{jseal}+R_p+R_{njseal}} V'_{msub}(j\omega) \approx \frac{R_{jseal}+R_{njseal}}{R_{jseal}+R_p+R_{njseal}} V'_{msub}(j\omega) \tag{M8}$$

$$V_{XAP}(j\omega) \approx \frac{R_{njseal}}{R_p+R_{njseal}} V'_{mAP}(j\omega) - \frac{R_p R_{jseal}}{R_p+R_{njseal}} C_{jm} \cdot j\omega V'_{mAP}(j\omega) \tag{M9}$$

The time-domain versions of equation (M8) and (M9) correspond to equation (9) and (10) in Table 1. $V_{Xsub}(j\omega)$ approximates to that in the single nanoprotrusion electrode case, whereas $V_{XAP}(j\omega)$ stays the same.

Regarding the recorded signal, with parameter substitutions in equation (6), we have $V_{in}(j\omega) = \frac{Z_{in}}{\tilde{Z}''_e+Z_{in}} V_X(j\omega)$, where $\tilde{Z}''_e = \frac{Z_e}{n} + \frac{R_{njseal}}{n} + R_{jseal}$.

3. Results and Discussion

By applying the analytical framework elaborated in *Methods* and *Supplementary Methods*, closed-form solutions are summarized in Table 1 for four recording configurations: extracellular and intracellular recordings using a single (Figure 2) or multiple (Figure 3) nanoprotrusion electrodes on the same planar microelectrode, respectively.

3.1 Extracellular and intracellular recordings using a single nanoprotrusion electrode

Let's consider the extracellular and intracellular recordings using a single nanoprotrusion electrode (Figure 2). For now, we assume that the substrate holding the nanoprotrusion electrode is passivated [4, 8] and will address the issue when the substrate-integrated microelectrode is exposed later on in the case of multiple nanoprotrusion electrodes. Our analyses are divided into two phases: subthreshold depolarization and AP, because the current sources for generating the transmembrane potential $V_m(j\omega)$ and the extracellular potential $V_X(j\omega)$ at the tip of the nanoprotrusion electrode in this two phases are fundamentally different. In subthreshold depolarization, the current source is an inward $I_{Stim}(j\omega)$ either injected externally or coming from synaptic inputs (or from passive dispersion from adjacent membrane AP, when propagation is considered), while during suprathreshold AP, the current source is the active transmembrane ionic currents (*e.g.*, in neurons, an inward $I_{Na}(j\omega)$ for depolarization, and an outward $I_K(j\omega)$ for repolarization) which function similar to a self-propelled battery. In each phase, $V_m(j\omega)$ and $V_X(j\omega)$ are linked by the net transmembrane current, so that we can derive

a relationship between them. We first consider that the nanoprotrusion electrode is completely insulated and thus ignore its equivalent circuit components in Figure 2, because the presence of the electrode recording circuit distorts the $V_X(j\omega)$ into $V_X'(j\omega)$, which will be discussed later. It should be noted that during the intracellular recording configurations after membrane poration, $V_m(j\omega)$ is slightly reduced to $V_m'(j\omega)$ due to transmembrane current leakage. By solving the equivalent electrical circuits in Figure 2 for $V_X(j\omega)$ as a function of $V_m(j\omega)$ (see *Methods*), we obtained analytical solutions for $V_X(j\omega)$ as described by equation (1)-(4) in Table 1. Under extracellular recording configuration, during subthreshold depolarization, $V_X(j\omega)$ is proportional to the first time derivative of $V_m(j\omega)$ (equation (1), unexpected); and during AP, $V_X(j\omega)$ is proportional to the *negative* first time derivative of the iAP $V_m(j\omega)$ (equation (2), agreeing with established knowledge). Under intracellular recording configuration, during subthreshold depolarization, $V_X(j\omega)$ is a fraction of $V_m'(j\omega)$ (equation (3)); and during AP, $V_X(j\omega)$ has two components: a fraction of the iAP $V_m'(j\omega)$ due to the leaking nanojunctional membrane and a fraction of the eFP at the junctional cleft due to the junctional membrane current (equation (4)), which were observed experimentally during the late resealing stage of the porated membrane when amplitudes of the two components were comparable [4]. However, shortly after membrane poration, as the amplitude of the first term is more than two orders of magnitude larger than that of the second (see Table 2 and *Supplementary Notes*), the overall $V_X(j\omega)$ looks like a scaled version of the iAP [4, 8, 11, 12]. In literature, these positive spikes are termed as "B-spike" [20] or "intracellular-like AP" [12], which is a reasonable description, as the signal is neither the full-stroke iAP, nor simply a scaled version of it, though their waveforms may look indiscernible.

Once the electrode recording circuit is present, the extracellular potential $V_X(j\omega)$ is distorted into $V_X'(j\omega)$ (see *Supplementary Methods 1.3*). For the specific configurations in Figure 2, $V_X'(j\omega)$ is related to $V_X(j\omega)$ by equation (5) in Table 1, indicating a slight magnitude attenuation. The electrode directly senses $V_X'(j\omega)$ through a voltage-divider circuit with an end result determined by equation (6), where the voltage $V_{in}(j\omega)$ appearing across input terminals of the AC amplifier is ultimately related to $V_X(j\omega)$ by substitution of $V_X'(j\omega)$ with equation (5) (see *Supplementary Methods*). Equation (6) indicates that the recorded signal $V_{in}(j\omega)$ is related to the pristine $V_X(j\omega)$ by a voltage-divider circuit, where the *in-situ* impedance Z_e'' of the nanoprotrusion electrode is cascaded with the input impedance Z_{in} of the amplifier. Note, the *in-situ* impedance Z_e'' is different from the conventional electrode impedance $Z_e' = Z_e + R_s$ as measured in an open electrolyte.

Unique to the nanoprotrusion electrode's recording situation, the electrode's recording impedance Z_e is high (*e.g.*, ~54 MΩ at 1 kHz [4]) due to its nano dimensions, and the *in-situ* series resistance $R_s' = R_{njseal} + R_{jseal}$ is very high (*e.g.*, > 900 MΩ [8]). According to equation (6), the amplifier's input impedance Z_{in} has to be even higher (*e.g.*, 1 GΩ [21]) in order to pick up a substantial fraction of $V_X(j\omega)$. In this case, $V_X'(j\omega)$ still approximates to $V_X(j\omega)$ (equation (5)), though the distortion becomes substantially larger than that could be caused by a microelectrode. Additionally, as Z_e becomes significant, the cutoff frequency of the highpass filter formed by the electrode's C_{dl} and the amplifier's input resistance can be raised by more than three orders of magnitude to above 50 Hz, which results in a $v_{in}(t)$ with a narrower temporal profile than that of the $v_X(t)$.

3.2 Recording by multiple nanoprotrusion electrodes on the same planar microelectrode

Our discussions above can be directly extended to multiple nanoprotrusion electrodes fabricated on the same planar microelectrode [4, 8, 12]. The equivalent electrical circuits with *n* nanoprotrusion electrodes are shown in Figure 3. If the surface of the planar microelectrode is passivated [4, 8], these circuits are the same as the those with only one nanoprotrusion electrode in Figure 2, except for a scaling factor *n* to the parameters in the nanojunction (see *Supplementary Methods*). The analytical solutions are summarized in Table 1.

For extracellular recording (equation (7) and (8)), $V_X(j\omega)$ is slightly enhanced but still approximates to that in the case of a single nanoprotrusion electrode, as *n* is usually small (*e.g.*, ≤ 9). This is because (i) the voltage across the nanojunctional resistance stays the same as the factor *n*'s in $nI_{Cnjm}(j\omega)$ or $-nI_{njm}(j\omega)$ and $\frac{R_{njseal}}{n}$ cancel with each other, and (ii) the additional current $(n-1)I_{Cnjm}(j\omega)$ or $-(n-1)I_{njm}(j\omega)$ (still very tiny due to the tiny β_{njm}) flowing through R_{jseal} only produces a tiny voltage increase in $V_{seal}(j\omega)$. After membrane poration, during subthreshold depolarization (equation (9)), $V_X(j\omega)$ is slightly enhanced but still approximates to that in the case of a single nanoprotrusion electrode, whereas during AP, $V_X(j\omega)$ stays the same as in the case of single nanoprotrusion electrode (equation (10)). In both configurations, the recorded signal $V_{in}(j\omega)$ is governed by equation (12). Interestingly, $V_{in}(j\omega)$ becomes substantially larger, as a result of reduction of the *in-situ* impedance Z_e'' of the nanoprotrusion electrode by approximately *n* times.

With an unpassivated substrate microelectrode surface [12, 22], the electric double layer capacitance C_{dl}' of the cell-covered electrode surface functions as a regular planar recording electrode to sense the extracellular potential $V_{seal}(j\omega)$ across R_{jseal}, which is superimposed onto the recorded $V_{in}(j\omega)$. However, unique to the intracellular configuration, $V_{seal}(j\omega)$ now has a small fraction of $V_m'(j\omega)$ due to the leaking current $nI_{njm}'(j\omega)$ from the nanojunctions,

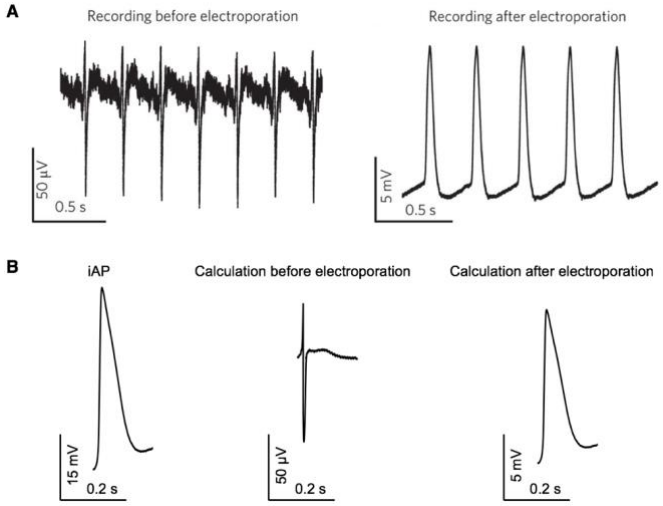

Figure 4. Comparison between empirical recordings and theoretical calculations. Nine nanoprotrusion electrodes fabricated on a passivated planar microelectrode were used to record from an HL-1 cell. (**A**), Empirical recordings as reported in Ref. [4]. (**B**), Theoretical calculations: left, an HL-1 cell iAP trace recorded using whole-cell patch clamp [23]; middle, calculated extracellular potential $v_x(t)$ according to equation (7) and (8) in Table 1; and right, calculated extracellular potential $v_x(t)$ according to equation (9) and (10). The AP threshold was set as 10 mV above the resting potential. Note that (i) the data in (**A**) are the non-deconvoluted $v_{in}(t)$ (equation (12)); (ii) (**A**) and (**B**) (left) were obtained from two different HL-1 cells in different conditions; and (iii) the exact parameters in equation (7)–(12) in the two experiments were unknown or incomplete. Thus, the conventional approach of overlapping the calculations on the recordings to show waveform matches [8, 12, 23, 25] is not used here. Figure reproduced with permission from: (**A**), Ref. [4], © 2012 NPG. Data courtesy with permission: (**B**), left, Ref. [23], Dr. Kristin H. Gilchrist.

which doesn't affect $V_{in}(j\omega)$ much as R_{jseal} is more than three orders of magnitude smaller than R_{njseal}.

Interestingly, if the cell only partially covers the microelectrode surface, the exposed electrode surface (modeled electrically by C''_{dl}) functions to shunt the effective input impedance of the amplifier, which has two effects: attenuating the magnitude of Z_{in} (*i.e.*, reducing the SNR of the recording according to equation (12)) and exerting a lowpass filtering effect. The larger the exposed electrode area, the worse these effects.

3.3 Validations with empirical results

These theoretical results are validated by fitting empirical data from literature to those equations in Table 1. In Figure 4, an iAP trace from an HL-1 cell (cardiac cell line) [23] is used to calculate the extracellular and intracellular recordings using nine nanoprotrusion electrodes fabricated on a passivated planar substrate microelectrode, and these calculations are compared to the empirical recordings in Ref. [4], showing a favorable waveform agreement. However, there are still some noticeable deviations. The recordings in Figure 4A were obtained from the edge of a pacemaker HL-1 cell [4]. The AP was initiated somewhere close to the center of the cell and propagated to the recording point at the edge, so the $I_{Stim}(j\omega)$ came from spreading of the forward-propagating AP current in the preceding membrane. But before this spreading $I_{Stim}(j\omega)$ arrived, the nanojunctional membrane had a slow, hyperpolarization-activated inward $I_{Ca}(j\omega)$ to depolarize the membrane, as shown in Figure 4A (right). It was this transmembrane $I_{Ca}(j\omega)$ generating the initial sag phase in Figure 4A (left), according to the negative first time derivative relationship governed by equation (2). Furthermore, during the repolarization phase, there should be a backward-propagated $I_{Stim}(j\omega)$ from the succeeding membrane AP current, which physically slowed down the repolarization and thus mathematically attenuated the first derivative of $V_m(j\omega)$, as seen in Figure 4B (middle) from a direct calculation. However, this $I_{Stim}(j\omega)$ did not attenuate the outward $I_K(j\omega)$ flowing into the extracellular space, rather, exited the membrane through the already opened K_+ channels and strengthened the outward $I_K(j\omega)$ to create a more prominent overshoot according to equation (2), as observed in Figure 4A (left). These two effects are not accounted in the calculation of the extracellular recording in Figure 4B (middle).

Furthermore, general agreements are also reached by an extensive comparison to empirical results in literature as shown in Table 2 (see *Supplementary Notes* for detailed calculations). The very low Z_{in} (*e.g.*, 1 MΩ || 9.45 nF [8]) of the amplifier used in some studies comparing to the Z'_e (*e.g.*, 54 MΩ at 1 kHz [4]) of the nanoprotrusion electrode and the shunting effect of the cell-uncovered, unpassivated planar microelectrode [12], which significantly attenuated the effective Z_{in}, could primarily account for the substantial differences between the recorded v_{in_peak} and calculated v_{X_peak}. It should be noted that without knowing the complete experimental details (such as the cell dimensions, how many percentage the cell body covered the unpassivated substrate microelectrode, and precise values of other key parameters), the calculated results are estimations and can only be interpreted qualitatively.

4. Conclusion

Through two key conceptual developments (see *Methods*), I advanced the equivalent electrical circuit model of the neuron-nanoelectrode interface to a critical level capable of deriving a closed-form analytical relationship between the transmembrane potential $V_m(j\omega)$ and extracellular potential $V_X(j\omega)$ during subthreshold depolarization and suprathreshold AP, respectively. Such closed-form solutions offer a clear and complete understanding on the recording mechanisms, nature of signals, and interplays between key interface parameters.

My analytical results show quantitively that the extracellular recording is proportional to the negative first time derivative of the iAP, whereas the intracellular-like recording contains portions of both the iAP and eFP. The

Table 2. Comparisons between empirical results in literature and theoretical estimations.

	# of electrodes	cell type	extracellular recording amplitude				intracellular recording amplitude				Z_e' and Z_{in} at 1 kHz	noise V_{pp} (μV)	Ref.
			AP (μV)		EPSP (μV)		AP (mV)		EPSP (mV)				
			experimental $v_{in}(t)$	calculated $v_X(t)$	experimental $v_{in}(t)$	calculated $v_X(t)$	experimental $v_{in}(t)$	calculated $v_X(t)$	experimental $v_{in}(t)$	calculated $v_X(t)$			
patch-clamp electrode	—	multiple	—	—	—	—	80-120	—	0.5-10	—	$\lvert Z_e'\rvert$: 1 MΩ	180*	[1],[4]
planar microelectrode†	—	neuron	-10 ~ -500	-33.7	—	1.9	—	—	—	—	$\lvert Z_e'\rvert$: 50 kΩ	10	[1],[4]
		HL-1 cell		-52.8		14.1							
gold mushroom-shaped microelectrode (gMμE)	1	Aplysia neurons	-200 ~ -300	-2552	—	255.2	0.5 ~ 25	19.8	5	4.0	$\lvert Z_{in}\rvert$: 20 MΩ		[16], [24], [25]
vertical nanowire electrode arrays (VNEA)‡	9	rat cortical neuron	—	—	—	—	4	26.6	—	3.0	Z_{in}: 1 MΩ ‖ 9.45 nF	200	[8]
platinum nanopillar electrode	9	HL-1 cell	-80	-101.5	—	27.1	11.8	22.2	—	3.0	$\lvert Z_e'\rvert$: 6 MΩ Z_{in}: 100 GΩ ‖ 10 pF	30	[4]
plasmonic nanopillar electrode§	1	rat hippocampal neuron	-100 ~ -400	-1465.9	100	81.4	0.6 ~ 1	26.6	0.04	3.0	Z_{in}: 13 MΩ ‖ 12 pF	40	[12]
	4	HL-1 cell	-400	-163.5	—	43.6	1.8	22.2	—	3.0		20	

*Current clamp recording mode, V_{rms}. †Diameter of electrode is 30 μm. ‡Faradaic recording regime is considered with a DC bias of -1.5 V. §The substrate microelectrode was unpassivated and taken into account. See *Supplementary Notes* for detailed calculations.

presence of multiple nanoprotrusion electrodes on the same conductive substrate only slightly increases the amplitude of $V_X(j\omega)$ comparing to the presence of a single electrode, however, the actual recording $V_{in}(j\omega)$ can be substantially improved as a result of reduction of the *in-situ* impedance Z_e'' of the nanoprotrusion electrode by approximately *n* times. Having the substrate unpassivated can distort the iAP component more with the eFP component, and the portion uncovered by cell can further severely compromise the recording quality.

This general theoretical framework is not configuration-specific and can be adapted to a variety of extracellular and intracellular recording situations, including using the vertical nanowire electrode arrays (VNEAs) in the 'Faradaic' regime [8], the gold plasmonic nanocylindrical electrode arrays with optoporation only at the electrode tips [12], and the gold mushroom-shaped microelectrode (gMμE) [16, 24, 25] (see Table 2 for examples). These findings have broad implications to advance the theory and practice of nano neurotechnologies, including offering critical insights to the proper design, characterization, and usage of this class of nanoelectrodes.

Acknowledgements

This work was supported by the National Science Foundation through Grant # 1749701 and the Defense Advanced Research Projects Agency through Grant # D17AP00031 of the USA. The views, opinions, and/or findings contained in this article are those of the author and should not be interpreted as representing the official views or policies, either expressed or implied, of the Defense Advanced Research Projects Agency or the Department of Defense. The author thanks Dr. Kristin H. Gilchrist for providing the HL-1 cell iAP data and Dr. Bianxiao Cui at Stanford University for communications on the data in Ref. [4]. The author also thanks Dr. Bozhi Tian at University of Chicago for commenting on a preliminary draft of the work.

References

[1] M. E. Spira and A. Hai, "Multi-electrode array technologies for neuroscience and cardiology," *Nature nanotechnology,* vol. 8, no. 2, pp. 83-94, 2013.

[2] J. S. Park *et al.*, "Intracellular cardiomyocytes potential recording by planar electrode array and fibroblasts co-culturing on multi-modal CMOS chip," *Biosensors and Bioelectronics,* vol. 144, p. 111626, 2019.

[3] M. Dipalo *et al.*, "Plasmonic meta-electrodes allow intracellular recordings at network level on high-density CMOS-multi-electrode arrays (vol 13, pg 965, 2018)," (in English), *Nature Nanotechnology,* vol. 13, no. 10, pp. 972-972, Oct 2018.

[4] C. Xie, Z. L. Lin, L. Hanson, Y. Cui, and B. X. Cui, "Intracellular recording of action potentials by nanopillar electroporation," (in English), *Nature Nanotechnology,* vol. 7, no. 3, pp. 185-190, Mar 2012.

[5] C. Xie, J. Liu, T. M. Fu, X. C. Dai, W. Zhou, and C. M. Lieber, "Three-dimensional macroporous nanoelectronic networks as minimally invasive brain probes," (in English), *Nature Materials,* vol. 14, no. 12, pp. 1286-1292, Dec 2015.

[6] T. Zhou *et al.*, "Syringe-injectable mesh electronics integrate seamlessly with minimal chronic immune response in the brain," *Proceedings of the National Academy of Sciences,* vol. 114, no. 23, pp. 5894-5899, 2017.

[7] T.-M. Fu, G. Hong, T. Zhou, T. G. Schuhmann, R. D. Viveros, and C. M. Lieber, "Stable long-term chronic brain mapping at the single-neuron level," *Nature methods,* vol. 13, no. 10, p. 875, 2016.

[8] J. T. Robinson, M. Jorgolli, A. K. Shalek, M. H. Yoon, R. S. Gertner, and H. Park, "Vertical nanowire electrode arrays as a scalable platform for intracellular interfacing to neuronal circuits," *Nat Nanotechnol,* vol. 7, no. 3, pp. 180-4, Jan 10 2012.

[9] B. Z. Tian, T. Cohen-Karni, Q. Qing, X. J. Duan, P. Xie, and C. M. Lieber, "Three-Dimensional, Flexible Nanoscale Field-Effect Transistors as Localized Bioprobes," (in English), *Science,* vol. 329, no. 5993, pp. 830-834, Aug 13 2010.

[10] Y. Wang *et al.*, "Nano functional neural interfaces," *Nano Research,* 2018.

[11] Z. L. C. Lin, C. Xie, Y. Osakada, Y. Cui, and B. X. Cui, "Iridium oxide nanotube electrodes for sensitive and prolonged intracellular measurement of action potentials," (in English), *Nature Communications,* vol. 5, Feb 2014.

[12] M. Dipalo *et al.*, "Intracellular and Extracellular Recording of Spontaneous Action Potentials in Mammalian Neurons and Cardiac Cells with 3D Plasmonic Nanoelectrodes," (in English), *Nano Letters,* vol. 17, no. 6, pp. 3932-3939, Jun 2017.

[13] C. Gold, D. A. Henze, C. Koch, and G. Buzsaki, "On the origin of the extracellular action potential waveform: A modeling study," *J Neurophysiol,* vol. 95, no. 5, pp. 3113-28, May 2006.

[14] M. Grattarola and S. Martinoia, "Modeling the neuron-microtransducer junction: from extracellular to patch recording," *IEEE Trans Biomed Eng,* vol. 40, no. 1, pp. 35-41, Jan 1993.

[15] P. Fromherz, "Electrical interfacing of nerve cells and semiconductor chips," (in English), *Chemphyschem,* vol. 3, no. 3, pp. 276-284, Mar 12 2002.

[16] A. Hai and M. E. Spira, "On-chip electroporation, membrane repair dynamics and transient in-cell recordings by arrays of gold mushroom-shaped microelectrodes," *Lab on a Chip,* vol. 12, no. 16, pp. 2865-2873, 2012.

[17] P. Massobrio, G. Massobrio, and S. Martinoia, "Interfacing Cultured Neurons to Microtransducers Arrays: A Review of the Neuro-Electronic Junction Models," (in English), *Frontiers in Neuroscience,* vol. 10, Jun 21 2016.

[18] M. K. Lewandowska, D. J. Bakkum, S. B. Rompani, and A. Hierlemann, "Recording large extracellular spikes in microchannels along many axonal sites from individual neurons," *PLoS One,* vol. 10, no. 3, p. e0118514, 2015.

[19] A. Oppenheim and A. Willsky, *Signals and Systems*, 2nd ed. Pearson, 1996.

[20] P. Fromherz, "Neuroeletrocnic Interfacing: Semiconductor Chips with Ion Channels, Nerve Cells and Brain, Nanoelectronics and Information Technology. 2003," *Wiley-VCH,* pp. 781-810.

[21] M. J. Nelson, P. Pouget, E. A. Nilsen, C. D. Patten, and J. D. Schall, "Review of signal distortion through metal microelectrode recording circuits and filters," (in English), *Journal of Neuroscience Methods,* vol. 169, no. 1, pp. 141-157, Mar 30 2008.

[22] M. Dipalo *et al.*, "Cells Adhering to 3D Vertical Nanostructures: Cell Membrane Reshaping without Stable Internalization," (in English), *Nano Letters,* vol. 18, no. 9, pp. 6100-6105, Sep 2018.

[23] K. H. Gilchrist, "Characterization and Validation of Cell-based Biosensors," Ph.D., Department of Electrical Engineering, Stanford University, 2003.

[24] A. Hai, J. Shappir, and M. E. Spira, "In-cell recordings by extracellular microelectrodes," (in English), *Nature Methods,* vol. 7, no. 3, pp. 200-U50, Mar 2010.

[25] A. Hai, J. Shappir, and M. E. Spira, "Long-Term, Multisite, Parallel, In-Cell Recording and Stimulation by an Array of Extracellular Microelectrodes," (in English), *Journal of Neurophysiology,* vol. 104, no. 1, pp. 559-568, Jul 2010.

Supplementary Material

On neural recording using nanoprotrusion electrodes

*Liang Guo**

Department of Electrical and Computer Engineering, Department of Neuroscience, The Ohio State University, Columbus, OH 43210, USA. *E-mail: guo.725@osu.edu.

1. Methods

1.1 The membrane-substrate junctional seal exerts a minimum effect on $I_{Cjm}(j\omega)$ in Figure 2A

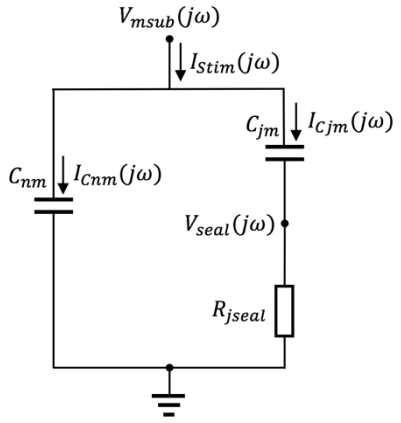

Figure S1. A reorganized circuit diagram of Figure 2A excluding the nanoprotrusion electrode.

Because $\omega C_{nm} R_{jseal} \ll \frac{C_{nm}}{C_{jm}}$ for $\omega \leq 2\pi \cdot 1$ kHz,

$$I_{Cjm}(j\omega) = \frac{\frac{1}{j\omega C_{nm}}}{\frac{1}{j\omega C_{nm}} + \left(\frac{1}{j\omega C_{jm}} + R_{jseal}\right)} I_{Stim}(j\omega) = \frac{1}{1 + \left(\frac{C_{nm}}{C_{jm}} + j\omega C_{nm} R_{jseal}\right)} I_{Stim}(j\omega)$$

$$\approx \frac{C_{jm}}{C_{nm} + C_{jm}} I_{Stim}(j\omega) = \beta_{jm} I_{Stim}(j\omega)$$

Therefore, $I_{Cjm}(j\omega)$ can be approximated as $\beta_{jm} I_{Stim}(j\omega)$, where β_{jm} is the percentage of the junctional membrane area to the entire cell membrane area, and the entire cell membrane can be considered to have a uniform transmembrane capacitive current density.

1.2 The nanojunctional seal exerts a minimum effect on $I_{Cnjm}(j\omega)$ in Figure 2A

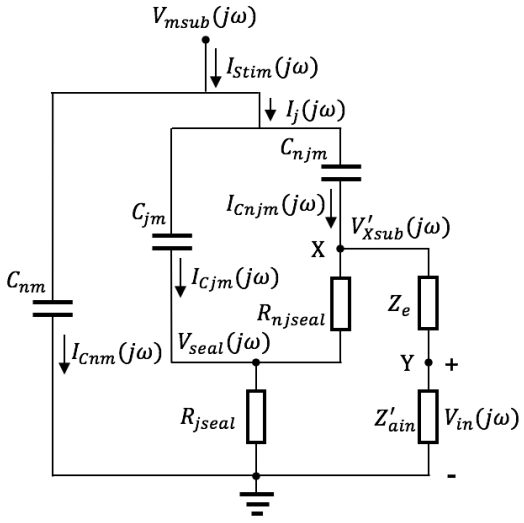

Figure S2. A reorganized circuit diagram of Figure 2A for better visualization.

In absence of the conductive electrode in Figure S2, because $\omega C_{jm} R_{njseal} \ll \frac{C_{jm}}{C_{njm}} \gg 1$ for $\omega \leq 2\pi \cdot 1$ kHz and $I_j(j\omega) = (\beta_{jm} + \beta_{njm}) I_{Stim}(j\omega) \approx \beta_{jm} I_{Stim}(j\omega)$,

$$I_{Cnjm}(j\omega) = \frac{\frac{1}{j\omega C_{jm}}}{\frac{1}{j\omega C_{jm}} + (\frac{1}{j\omega C_{njm}} + R_{njseal})} I_j(j\omega) = \frac{1}{1 + (\frac{C_{jm}}{C_{njm}} + j\omega C_{jm} R_{njseal})} I_j(j\omega) \approx \frac{C_{njm}}{C_{jm}} I_j(j\omega)$$

$$= \frac{\beta_{njm}}{\beta_{jm}} I_j(j\omega) \approx \beta_{njm} I_{Stim}(j\omega)$$

Therefore, $I_{Cnjm}(j\omega)$ can be approximated as $\beta_{njm} I_{Stim}(j\omega)$, where β_{njm} is the percentage of the nanojunctional membrane area to the entire cell membrane area, and the entire cell membrane can be considered to have a uniform transmembrane capacitive current density.

1.3 Derivation of equations (5) and (6) in Table 1

In Figure 2A,

$$V'_{Xsub}(j\omega) = \frac{(Z_e + Z_{in})(R_{njseal} + R_{jseal})}{Z_e + Z'_{ain} + R_{njseal} + R_{jseal}} I_{Cnjm}(j\omega) + \frac{(R_{njseal} + Z_e + Z_{in}) R_{jseal}}{R_{njseal} + Z_e + Z'_{ain} + R_{jseal}} I_{Cjm}(j\omega) \frac{Z_e + Z_{in}}{R_{njseal} + Z_e + Z_{in}}$$

$$= \frac{(Z_e + Z_{in})(R_{njseal} + R_{jseal})}{Z_e + Z_{in} + R_{njseal} + R_{jseal}} I_{Cnjm}(j\omega) + \frac{(Z_e + Z_{in}) R_{jseal}}{R_{njseal} + Z_e + Z_{in} + R_{jseal}} I_{Cjm}(j\omega)$$

$$= \frac{Z_e + Z_{in}}{Z_e + Z_{in} + R_{njseal} + R_{jseal}} \left((R_{njseal} + R_{jseal}) I_{Cnjm}(j\omega) + R_{jseal} I_{Cjm}(j\omega) \right)$$

$$= \frac{Z_e + Z_{in}}{Z_e + Z_{in} + R_{njseal} + R_{jseal}} V_{Xsub}(j\omega)$$

$$V_{in}(j\omega) = \frac{Z_{in}}{Z_e + Z_{in}} V'_{Xsub}(j\omega) = \frac{Z_{in}}{Z_e + Z_{in}} \cdot \frac{Z_e + Z_{in}}{Z_e + Z_{in} + R_{njseal} + R_{jseal}} V_{Xsub}(j\omega)$$

$$= \frac{Z_{in}}{Z_e + Z_{in} + R_{njseal} + R_{jseal}} V_{Xsub}(j\omega)$$

Derivations of $V'_X(j\omega)$ and $V_{in}(j\omega)$ in Figures 2B, 2C, and 2D are similar and have the same results. Therefore,

$$V'_X(j\omega) = \frac{1}{1 + \frac{R'_s}{Z_e + Z_{in}}} V_X(j\omega)$$

$$V_{in}(j\omega) = \frac{Z_{in}}{Z''_e + Z_{in}} V_X(j\omega)$$

where $R'_s = R_{njseal} + R_{jseal}$, and $Z''_e = Z_e + R'_s$.

1.4 Solving the circuit in Figure 2C for $V_{Xsub}(j\omega)$

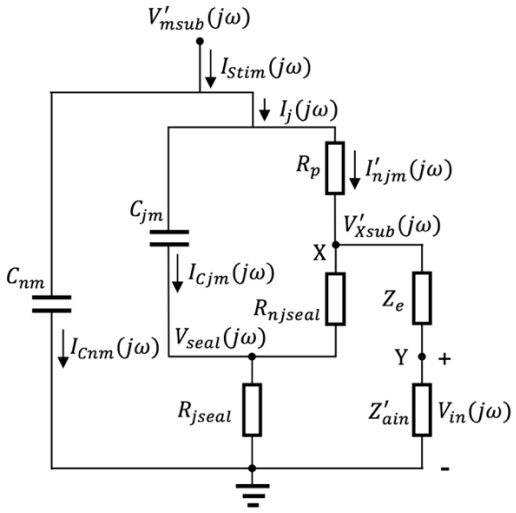

Figure S3. A reorganized circuit diagram of Figure 2C for better visualization.

In absence of the electrode in Figure S3,

$$V_{seal}(j\omega) = \frac{R_{jseal}}{R_{jseal} + \dfrac{(R_p + R_{njseal})\dfrac{1}{j\omega C_{jm}}}{R_p + R_{njseal} + \dfrac{1}{j\omega C_{jm}}}} V'_{msub}(j\omega) = \frac{R_{jseal}}{R_{jseal} + \dfrac{R_p + R_{njseal}}{j\omega C_{jm}(R_p + R_{njseal}) + 1}} V'_{msub}(j\omega)$$

$$= \frac{R_{jseal}[j\omega C_{jm}(R_p + R_{njseal}) + 1]}{R_{jseal}[j\omega C_{jm}(R_p + R_{njseal}) + 1] + R_p + R_{njseal}} V'_{msub}(j\omega)$$

$$= \frac{R_{jseal}[j\omega C_{jm}(R_p + R_{njseal}) + 1]}{j\omega C_{jm} R_{jseal}(R_p + R_{njseal}) + R_{jseal} + R_p + R_{njseal}} V'_{msub}(j\omega)$$

$$V_{Xsub}(j\omega) = \frac{R_{njseal}}{R_p + R_{njseal}}\left(V'_{msub}(j\omega) - V_{seal}(j\omega)\right) + V_{seal}(j\omega) = \frac{R_{njseal}}{R_p + R_{njseal}} V'_{msub}(j\omega) + \frac{R_p}{R_p + R_{njseal}} V_{seal}(j\omega)$$

$$= \frac{R_{njseal}}{R_p + R_{njseal}} V'_{msub}(j\omega) + \frac{R_p}{R_p + R_{njseal}} \cdot \frac{R_{jseal}\left[j\omega C_{jm}\left(R_p + R_{njseal}\right) + 1\right]}{j\omega C_{jm} R_{jseal}\left(R_p + R_{njseal}\right) + R_{jseal} + R_p + R_{njseal}} V'_{msub}(j\omega)$$

$$= \frac{1}{R_p + R_{njseal}} \cdot \left(R_{njseal} + \frac{R_p R_{jseal}\left[j\omega C_{jm}\left(R_p + R_{njseal}\right) + 1\right]}{j\omega C_{jm} R_{jseal}\left(R_p + R_{njseal}\right) + R_{jseal} + R_p + R_{njseal}} \right) V'_{msub}(j\omega)$$

$$= \frac{1}{R_p + R_{njseal}} \cdot \left(R_{njseal} + R_p - \frac{R_p\left(R_p + R_{njseal}\right)}{j\omega C_{jm} R_{jseal}\left(R_p + R_{njseal}\right) + R_{jseal} + R_p + R_{njseal}} \right) V'_{msub}(j\omega)$$

$$= \left(1 - \frac{R_p}{j\omega C_{jm} R_{jseal}\left(R_p + R_{njseal}\right) + R_{jseal} + R_p + R_{njseal}} \right) V'_{msub}(j\omega)$$

$$= \left(1 - \frac{\dfrac{R_p}{R_{jseal} + R_p + R_{njseal}}}{j\omega \dfrac{C_{jm} R_{jseal}\left(R_p + R_{njseal}\right)}{R_{jseal} + R_p + R_{njseal}} + 1} \right) V'_{msub}(j\omega)$$

1.5 Solving the circuit in Figure 2D for $V_{XAP}(j\omega)$

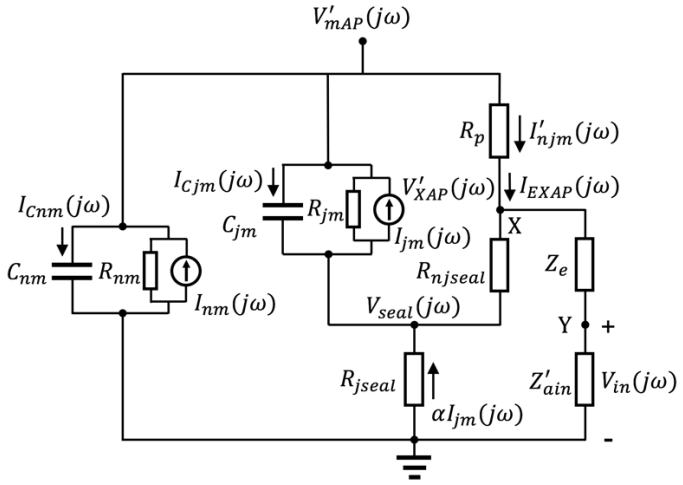

Figure S4. A reorganized circuit diagram of Figure 2D for better visualization.

In absence of the electrode in Figure S4,

$$I_{Cnm}(j\omega) + I_{Cjm}(j\omega) = I_{nm}(j\omega) + I_{jm}(j\omega) - I'_{njm}(j\omega) \Longrightarrow$$

$$C_{nm} \cdot j\omega V'_{mAP}(j\omega) + C_{jm} \cdot j\omega\big(V'_{mAP}(j\omega) - V_{seal}(j\omega)\big) = I_{nm}(j\omega) + I_{jm}(j\omega) - (1-\alpha)I_{jm}(j\omega) \Longrightarrow$$

$$j\omega\big(C_{nm} + C_{jm}\big)V'_{mAP}(j\omega) + j\omega C_{jm}R_{jseal}\alpha I_{jm}(j\omega) = \left(\frac{\beta_{nm}}{\beta_{jm}} + \alpha\right) I_{jm}(j\omega) \Longrightarrow$$

$$j\omega\big(C_{nm} + C_{jm}\big)V'_{mAP}(j\omega) = \left(\frac{\beta_{nm}}{\beta_{jm}} + \alpha(1 - j\omega C_{jm}R_{jseal})\right) I_{jm}(j\omega) \Longrightarrow$$

$$I_{jm}(j\omega) = \frac{j\omega\big(C_{nm} + C_{jm}\big)}{\frac{\beta_{nm}}{\beta_{jm}} + \alpha(1 - j\omega C_{jm}R_{jseal})} V'_{mAP}(j\omega)$$

$$V'_{mAP}(j\omega) = \big(R_p + R_{njseal}\big)I'_{njm}(j\omega) - R_{jseal}\alpha I_{jm}(j\omega) = \big(R_p + R_{njseal}\big)(1-\alpha)I_{jm}(j\omega) - R_{jseal}\alpha I_{jm}(j\omega)$$

$$= \Big(\big(R_p + R_{njseal}\big) - \alpha\big(R_p + R_{njseal} + R_{jseal}\big)\Big) I_{jm}(j\omega)$$

$$= \Big(\big(R_p + R_{njseal}\big) - \alpha\big(R_p + R_{njseal} + R_{jseal}\big)\Big) \frac{j\omega\big(C_{nm} + C_{jm}\big)}{\frac{\beta_{nm}}{\beta_{jm}} + \alpha(1 - j\omega C_{jm}R_{jseal})} V'_{mAP}(j\omega) \Longrightarrow$$

$$\Big(\big(R_p + R_{njseal}\big) - \alpha\big(R_p + R_{njseal} + R_{jseal}\big)\Big) \frac{j\omega\big(C_{nm} + C_{jm}\big)}{\frac{\beta_{nm}}{\beta_{jm}} + \alpha(1 - j\omega C_{jm}R_{jseal})} = 1 \Longrightarrow$$

$$j\omega\big(C_{nm} + C_{jm}\big)\Big(\big(R_p + R_{njseal}\big) - \alpha\big(R_p + R_{njseal} + R_{jseal}\big)\Big) = \frac{\beta_{nm}}{\beta_{jm}} + \alpha\big(1 - j\omega C_{jm}R_{jseal}\big) \Longrightarrow$$

$$j\omega\big(C_{nm} + C_{jm}\big)\big(R_p + R_{njseal}\big) - \frac{\beta_{nm}}{\beta_{jm}} = \alpha\Big(j\omega\big(C_{nm} + C_{jm}\big)\big(R_p + R_{njseal} + R_{jseal}\big) + \big(1 - j\omega C_{jm}R_{jseal}\big)\Big) \Longrightarrow$$

$$\alpha = \frac{j\omega\left(C_{nm}+C_{jm}\right)\left(R_p+R_{njseal}\right)-\frac{\beta_{nm}}{\beta_{jm}}}{j\omega\left(C_{nm}+C_{jm}\right)\left(R_p+R_{njseal}+R_{jseal}\right)+1-j\omega C_{jm}R_{jseal}} \approx \frac{R_p+R_{njseal}}{R_p+R_{njseal}+R_{jseal}} \approx 1$$

$$I'_{njm}(j\omega) = (1-\alpha)I_{jm}(j\omega) \approx \frac{R_{jseal}}{R_p+R_{njseal}+R_{jseal}} I_{jm}(j\omega)$$

$$V_{seal}(j\omega) = -R_{jseal}\alpha I_{jm}(j\omega)$$

$$V_{XAP}(j\omega) = \frac{R_{njseal}}{R_p+R_{njseal}}\left(V'_{mAP}(j\omega)-V_{seal}(j\omega)\right)+V_{seal}(j\omega) = \frac{R_{njseal}}{R_p+R_{njseal}}V'_{mAP}(j\omega)+\frac{R_p}{R_p+R_{njseal}}V_{seal}(j\omega)$$

$$= \frac{R_{njseal}}{R_p+R_{njseal}}V'_{mAP}(j\omega)-\frac{R_p}{R_p+R_{njseal}}R_{jseal}\alpha I_{jm}(j\omega)$$

$$= \frac{R_{njseal}}{R_p+R_{njseal}}V'_{mAP}(j\omega)-\frac{R_p}{R_p+R_{njseal}}R_{jseal}\alpha\frac{j\omega\left(C_{nm}+C_{jm}\right)}{\frac{\beta_{nm}}{\beta_{jm}}+\alpha\left(1-j\omega C_{jm}R_{jseal}\right)}V'_{mAP}(j\omega)$$

$$= \frac{R_{njseal}}{R_p+R_{njseal}}V'_{mAP}(j\omega)-\frac{R_pR_{jseal}}{R_p+R_{njseal}}\cdot\frac{j\omega\left(C_{nm}+C_{jm}\right)}{\frac{\beta_{nm}}{\alpha\beta_{jm}}+\left(1-j\omega C_{jm}R_{jseal}\right)}V'_{mAP}(j\omega)$$

$$\approx \frac{R_{njseal}}{R_p+R_{njseal}}V'_{mAP}(j\omega)-\frac{R_pR_{jseal}}{R_p+R_{njseal}}\cdot j\omega\frac{\beta_{jm}}{\beta_{nm}+\beta_{jm}}\left(C_{nm}+C_{jm}\right)V'_{mAP}(j\omega)$$

$$= \frac{R_{njseal}}{R_p+R_{njseal}}V'_{mAP}(j\omega)-\frac{R_pR_{jseal}}{R_p+R_{njseal}}C_{jm}\cdot j\omega V'_{mAP}(j\omega)$$

1.6 Derivation of the multi-nanoprotrusion electrode model in Figure 3

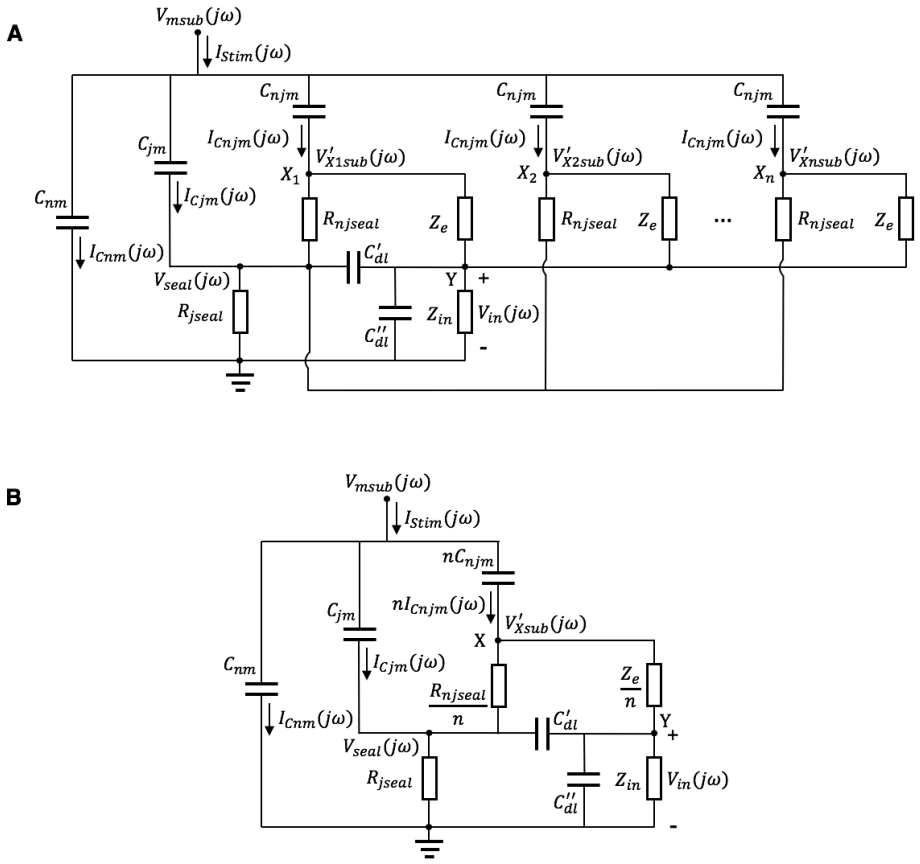

Figure S5. The multi-nanoprotrusion electrode model in (**A**) is equivalent to that in (**B**).

For n identical nanoprotrusion electrodes densely packed on the same planar microelectrode (Figure S5A), the potentials at Point X_n's are identical, i.e., $V'_{X1sub}(j\omega) = V'_{X2sub}(j\omega) = \cdots = V'_{Xnsub}(j\omega)$. Thus, the C_{njm}'s, R_{njseal}'s and Z_e's are in parallel with each other, which leads to the equivalent model in Figure S5B that is a reorganized circuit diagram of that in Figure 3A. The equivalent circuit models in Figure 3B, 3C and 3D are derived similarly.

2. Notes

Detailed calculations for $v_X(t)$ in Table 2

Parameters used for calculations

General:

Specific membrane capacitance: $C_{ms} = 0.01\ \mathrm{pF/\mu m^2}$

Series resistance from a planar microelectrode surface: $R_s = 2\ \mathrm{k\Omega}$

Neuron:

Rat cortical neuron: $r = 7.5$ μm, $C_{jm} = 1.77$ pF, $C_{nm} = 3.53$ pF, $C_{njm} = 0.01$ pF, $C_m = 5.3$ pF, $R_{jseal} = 0.1$ MΩ, rising phase $\frac{\Delta v_{mAP}}{\Delta t} = \frac{90\ mV}{0.5\ ms} = 180\ V/s$, $\frac{\Delta v_{msub}}{\Delta t} = \frac{10\ mV}{1\ ms} = 10\ V/s$

HL-1 Cell:
$A_{njm} = 0.724\ \mu m^2$, $A_{jm} = 1000\ \mu m^2$, $A_{jm}: A_{nm} = 3:4$ => $C_{njm} = 0.00724$ pF, $C_{jm} = 10$ pF, $C_m = 23.3$ pF, $R_{jseal} = 0.7$ MΩ, rising phase (pacemaker cell) $\frac{\Delta v_{mAP}}{\Delta t} = \frac{75\ mV}{10\ ms} = 7.5\ V/s$, $\frac{\Delta v_{msub}}{\Delta t} = \frac{10\ mV}{5\ ms} = 2\ V/s$

Planar microelectrode

In equation (1) and (2) in Table 1, assume $\beta_{njm} = 0$ and $R_s \neq 0$, then we have

$v_{Xsub}(t) = (\beta_{jm}R_{jseal} + R_s)C_m \cdot \frac{dv_{msub}(t)}{dt}$, $\quad v_{XAP}(t) = -(\beta_{jm}R_{jseal} + R_s)C_m \cdot \frac{dv_{mAP}(t)}{dt}$

HL-1 Cell:

$$v_{Xsub\_peak} = \left(\frac{3}{7} \times 0.7\ M\Omega + 2\ \text{k}\Omega\right) \times 23.3\ pF \times 2\frac{V}{s} = 14.1\ \mu\text{V}$$

$$v_{XAP\_peak} = -\left(\tfrac{3}{7} \times 0.7\ M\Omega + 2\ \text{k}\Omega\right) \times 23.3\ pF \times 7.5\tfrac{V}{s} = -52.8\ \mu\text{V}$$

Neuron:

$$v_{Xsub\_peak} = \left(\frac{1}{3} \times 0.1\ M\Omega + 2\ \text{k}\Omega\right) \times 5.3\ pF \times 10\frac{V}{s} = 1.9\ \mu\text{V}$$

$$v_{XAP\_peak} = -\left(\tfrac{1}{3} \times 0.1\ M\Omega + 2\ \text{k}\Omega\right) \times 5.3\ pF \times 180\tfrac{V}{s} = -33.7\ \mu\text{V}$$

Gold mushroom-shaped microelectrode (gMμE)

Cell type: Aplysia neuron, $r = 25$ μm, $n = 1$, $R_{njseal} + R_{jseal} = 67$ MΩ, $R_{jseal} = 1.2$ MΩ, $R_{njseal} = 65.8$ MΩ, $R_p = 100$ MΩ, $A_{njm} = 14\ \mu m^2$, $C_{njm} = 0.1$ pF, $C_m = 78.5$ pF, $C_{nm} = 62.8$ pF, $C_{jm} = 15.7$ pF, $\beta_{njm} = 0.00127$, $\beta_{jm} = \frac{1}{5}$, rising phase $\frac{\Delta v_{mAP}}{\Delta t} = \frac{50\ mV}{0.5\ ms} = 100\ V/s$, $\frac{\Delta v_{msub}}{\Delta t} = \frac{10\ mV}{1\ ms} = 10\ V/s$

Extracellular (PLL coating)

$$v_{Xsub\_peak} \approx \left[\beta_{njm}R_{njseal} + (\beta_{jm} + \beta_{njm})R_{jseal}\right]C_m \cdot \frac{dv_{msub}(t)}{dt}$$

$$= \left[0.00127 \times 65.8 + \left(\frac{1}{5} + 0.00127\right) \times 1.2\right] \times 78.5\ \times 10 = 255.2\ \mu\text{V}$$

$$v_{XAP\_peak} = -\left[\beta_{njm}R_{njseal} + (\beta_{jm} + \beta_{njm})R_{jseal}\right]C_m \cdot \frac{dv_{mAP}(t)}{dt} = -2552\ \mu\text{V}$$

Intracellular-like

PLL coating, electroporation

$$v_{Xsub\_peak} = \frac{R_{jseal} + R_{njseal}}{R_{jseal} + R_p + R_{njseal}} v'_{msub\_peak} = \frac{67}{167} \times 10 \text{ mV} = 4.012 \text{ mV}$$

According to equation (4) in Table 1, $v_{XAP}(t) \approx \frac{R_{njseal}}{R_p + R_{njseal}} v'_{mAP}(t) - \frac{R_p R_{jseal}}{R_p + R_{njseal}} C_{jm} \cdot \frac{dv'_{mAP}(t)}{dt}$. However, $\frac{dv'_{mAP}(t)}{dt} = 0$ at $v'_{mAP\_peak}(t)$, so

$$v_{XAP\_peak} \approx \frac{R_{njseal}}{R_p + R_{njseal}} v'_{mAP\_peak} = \frac{65.8}{165.8} \times 50 \text{ mV} = 19.8432 \text{ mV}$$

EPP coating, no electroporation, equivalent to superposition of the extracellular and intracellular situations above, however, the extracellular field potential is 0 at $v'_{mAP\_peak}(t)$, so that the overall peak values equal to those of the intracellular-like recordings: $v_{Xsub\_peak}(t) = 4.012$ mV and $v_{XAP\_peak}(t) = 19.8432\ mV$.

Vertical nanowire electrode array (VNEA)

Only the intracellular Faradaic regime is considered here, because of sufficient data provided in the paper. In this current-clamp mode, the only difference from our AC models in Figure 2 and Figure 3 is that a parallel Faradaic resistance R_f to C_{dl} is present in the nanoprotrusion electrode's electric double layer model.

Cell type: rat cortical neuron. Nanoprotrusion electrode: 150 nm diameter, 3 μm height, exposed height 1.2 μm, $n = 9$, $C_{dl} = 2.4$ pF.

The unporated nanojunctional membrane needs to be considered as an additional contribution to $v_X(t)$. $A_{njm\_p} = 0.5829$ μm^2, $A_{njm\_up} = 0.8478$ μm^2, $A_m = 530$ μm^2 => $\beta_{njm\_p} = 0.0011$, $\beta_{njm\_up} = 0.0016$, $R_e = 20$ kΩ (estimated). $\frac{R_{njseal}}{9} + R_{jseal} = 100$ MΩ => $R_{njseal} = 900$ MΩ. $\frac{R_p + R_f + R_e}{9} = 300$ MΩ, $\frac{R_f + R_e}{9} = 62$ MΩ => $R_p = 2142$ MΩ, $R_f = 558$ MΩ at -1.5 V bias with an RC time constant of 9.3 ms and parasitic capacitance of 150 pF. Amplifier's input resistance: $R_{in} = 1$ MΩ (Axon Digidata 1322A, Molecular Devices).

Recalculated parasitic capacitance at the amplifier input terminal $C_g = \frac{\tau}{\frac{R_f + R_e}{9} \,||\, R_{in} \,||\, R_L} = \frac{9.3 \text{ ms}}{62 \text{ MΩ} \,||\, 1\text{MΩ} \,||\, 1.5 \text{ GΩ}} = 9.45$ nF.

$$v_{Xsub}(t)|_{n=9} = \frac{nR_{jseal} + R_{njseal}}{nR_{jseal} + R_p + R_{njseal}} v'_{msub}(t) + \left[\beta_{njm\_up} R_{njseal} + \left(\beta_{jm} + n\beta_{njm\_up}\right) R_{jseal}\right] C_m \cdot \frac{dv'_{msub}(t)}{dt}$$

However, $\frac{dv'_{msub}(t)}{dt} = 0$ at v'_{msub_peak}, so

$$v_{Xsub\_peak}\big|_{n=9} = \frac{nR_{jseal} + R_{njseal}}{nR_{jseal} + R_p + R_{njseal}} v'_{msub\_peak} = \frac{9 \times 0.1 + 900}{9 \times 0.1 + 2142 + 900} \times 10 \text{ mV} = 2.9607 \text{ mV}$$

For comparison with only one nanoprotrusion electrode: $v_{Xsub\_peak}\big|_{n=1} = \frac{R_{jseal}+R_{njseal}}{R_{jseal}+R_p+R_{njseal}} v'_{msub\_peak} = 2.9588$ mV.

$$v_{XAP}(t) \approx \frac{R_{njseal}}{R_p + R_{njseal}} v'_{mAP}(t) - \frac{R_p R_{jseal}}{R_p + R_{njseal}} C_{jm} \cdot \frac{dv'_{mAP}(t)}{dt} - \left[\beta_{njm_{up}} R_{njseal} + \left(\beta_{jm} + n\beta_{njm_{up}}\right) R_{jseal}\right] C_m \cdot \frac{dv'_{mAP}(t)}{dt}$$

As $\frac{dv'_{mAP}(t)}{dt} = 0$ at v'_{mAP_peak},

$$v_{XAP\_peak} \approx \frac{R_{njseal}}{R_p + R_{njseal}} v'_{mAP\_peak} = \frac{900}{2142 + 900} \times 90 \text{ mV} = 26.6272 \text{ mV}$$

Platinum nanopillar electrode

Cell type: HL-1 cell, $n = 9$, $\beta_{njm} = 0.00031$, $\beta_{jm} = 0.428571$, $R_{njseal} = 900$ MΩ, $R_p = 2142$ MΩ. Single electrode $|Z'_e|_{f=1\,kHz} = 54$ MΩ, $A_e = 0.724$ μm^2.

Extracellular

$$v_{Xsub\_peak}\big|_{n=9} \approx \left[\beta_{njm} R_{njseal} + \left(\beta_{jm} + n\beta_{njm}\right) R_{jseal}\right] C_m \cdot \frac{dv_{msub}(t)}{dt}$$
$$= [0.00031 \times 900\ M\Omega + (0.428571 + 9 \times 0.00031) \times 0.7 \text{ MΩ}] \times 23.3\ pF \times 2\frac{V}{s}$$
$$= [0.279\ M\Omega + 0.302 \text{ MΩ}] \times 23.3\ pF \times 2\frac{V}{s} = 27.0746 \text{ μV}$$

For comparison with only one nanoprotrusion electrode:

$$v_{Xsub\_peak}\big|_{n=1} \approx \left[\beta_{njm} R_{njseal} + \left(\beta_{jm} + \beta_{njm}\right) R_{jseal}\right] C_m \cdot \frac{dv_{msub}(t)}{dt} = 26.9814 \text{ μV}$$

$$v_{XAP\_peak}\big|_{n=9} = -\left[\beta_{njm} R_{njseal} + \left(\beta_{jm} + n\beta_{njm}\right) R_{jseal}\right] C_m \cdot \frac{dv_{mAP}(t)}{dt}$$
$$= -[0.00031 \times 900\ M\Omega + (0.428571 + 9 \times 0.00031) \times 0.7 \text{ MΩ}] \times 23.3\ pF \times 7.5\frac{V}{s} = -101.5215 \text{ μV}$$

$$v_{XAP\_peak}\big|_{n=1} = -\left[\beta_{njm} R_{njseal} + \left(\beta_{jm} + \beta_{njm}\right) R_{jseal}\right] C_m \cdot \frac{dv_{mAP}(t)}{dt} = -101.2181 \text{ μV}$$

Intracellular-like

$$v_{Xsub\_peak}\big|_{n=9} = \frac{nR_{jseal} + R_{njseal}}{nR_{jseal} + R_p + R_{njseal}} v'_{msub\_peak} = \frac{9 \times 0.7 + 900}{9 \times 0.7 + 2142 + 900} \times 10\ mV$$
$$= 2.9731 \text{ mV}$$

$$v_{Xsub\_peak}\big|_{n=1} = \frac{R_{jseal} + R_{njseal}}{R_{jseal} + R_p + R_{njseal}} v'_{msub\_peak} = 2.9602 \text{ mV}$$

$v_{XAP}(t) \approx \frac{R_{njseal}}{R_p+R_{njseal}} v'_{mAP}(t) - \frac{R_p R_{jseal}}{R_p+R_{njseal}} C_{jm} \cdot \frac{dv'_{mAP}(t)}{dt}$, doesn't depend on the number of nanoprotrusion electrodes. As $\frac{dv'_{mAP}(t)}{dt} = 0$ at v'_{mAP_peak},

$$v_{XAP\_peak} \approx \frac{R_{njseal}}{R_p + R_{njseal}} v'_{mAP\_peak} = \frac{900}{2142 + 900} \times 75 \text{ mV} = 22.1893 \text{ mV}$$

Thus, enhancement to the signal $v_X(t)$ itself by using multiple nanoprotrusion electrodes is minimum. But, more nanoprotrusion electrodes can have a more prominent effect on improving the recorded $v_{in}(t)$ according to equation (12) in Table 1.

Plasmonic nanopillar electrode

The planar substrate microelectrode was unpassivated. Nanopores were only opened at the tip of the pillar by plasmonic optoporation, making R_p higher. The unporated nanojunctional membrane needs to be considered as an additional contribution to $v_X(t)$.

Rat hippocampal neuron:

Electrode: $n = 1$, 150 nm diameter, 1.8 μm height, $A_{njm} = 0.8655$ μm^2, $C_{njm} = 0.008655$ pF, $C_m = 5.3$ pF. $\beta_{njm} = 0.001633$, $\beta_{jm} = \frac{1}{3}$, planar microelectrode diameter 5 μm.

$v_{Xsub}(t) = \beta_{jm} R_{jseal} C_m \cdot \frac{dv_{msub}(t)}{dt}$

$v_{XAP}(t) = -\beta_{jm} R_{jseal} C_m \cdot \frac{dv_{mAP}(t)}{dt}$

$v_{Xsub\_peak} = \frac{1}{3} \times 0.1\ M\Omega \times 5.3\ pF \times 10 \frac{V}{s} = 1.77$ μV

$v_{XAP\_peak} = -\frac{1}{3} \times 0.1\ M\Omega \times 5.3\ pF \times 180 \frac{V}{s} = -31.8$ μV

Extracellular

$$v_{Xsub}(t) \approx \left[\beta_{njm} R_{njseal} + \left(\beta_{jm} + \beta_{njm}\right) R_{jseal}\right] C_m \cdot \frac{dv_{msub}(t)}{dt} + \beta_{jm} R_{jseal} C_m \cdot \frac{dv_{msub}(t)}{dt}$$
$$= \left[0.001633 \times 900\ M\Omega + \left(\frac{1}{3} + 0.001633\right) \times 0.1\ \text{M}\Omega\right] \times 5.3\ pF \times 10 \frac{V}{s} + 1.77\ \mu\text{V}$$
$$= 79.67 + 1.77 = 81.44\ \mu\text{V}$$

$$v_{XAP}(t) = -\left[\beta_{njm} R_{njseal} + \left(\beta_{jm} + \beta_{njm}\right) R_{jseal}\right] C_m \cdot \frac{dv_{mAP}(t)}{dt} - \beta_{jm} R_{jseal} C_m \cdot \frac{dv_{mAP}(t)}{dt}$$
$$= -1434.1 - 31.8 = -1465.9\ \mu\text{V}$$

Intracellular-like

$A_{njm\_p} = 0.0177$ μm^2, $A_{njm\_up} = 0.8478$ μm^2, $A_m = 530$ μm^2 => $\beta_{njm\_p} = 0.0000334$, $\beta_{njm\_up} = 0.0016$.

$$v_{Xsub}(t) = \frac{R_{jseal} + R_{njseal}}{R_{jseal} + R_p + R_{njseal}} v'_{msub}(t) + \left[\beta_{njm\_up} R_{njseal} + \left(\beta_{jm} + \beta_{njm\_up}\right) R_{jseal}\right] C_m \cdot \frac{dv'_{msub}(t)}{dt} + \beta_{jm} R_{jseal} C_m \cdot \frac{dv'_{msub}(t)}{dt}$$

Thus,

$$v_{Xsub\_peak} = \frac{R_{jseal} + R_{njseal}}{R_{jseal} + R_p + R_{njseal}} v'_{msub\_peak} = \frac{0.1 + 900}{0.1 + 2142 + 900} \times 10 \text{ mV} = 2.9588 \text{ mV}$$

$$v_{XAP}(t) \approx \frac{R_{njseal}}{R_p + R_{njseal}} v'_{mAP}(t) - \frac{R_p R_{jseal}}{R_p + R_{njseal}} C_{jm} \cdot \frac{dv'_{mAP}(t)}{dt} - \left[\beta_{njm_{up}} R_{njseal} + \left(\beta_{jm} + \beta_{njm_{up}}\right) R_{jseal}\right] C_m \cdot \frac{dv'_{mAP}(t)}{dt} - \beta_{jm} R_{jseal} C_m \cdot \frac{dv_{mAP}(t)}{dt}$$

Thus,

$$v_{XAP\_peak} \approx \frac{R_{njseal}}{R_p + R_{njseal}} v'_{mAP\_peak} = \frac{900}{2142 + 900} \times 90 \text{ mV} = 26.6272 \text{ mV}$$

HL-1 cell:

$n = 4$, $A_{njm} = 0.8655\ \mu\text{m}^2$, $A_{njm\_p} = 0.0177\ \mu\text{m}^2$, $A_{njm\_up} = 0.8478\ \mu\text{m}^2$, $A_m = 2330\ \mu\text{m}^2$ => $\beta_{njm} = 0.0003715$, $\beta_{njm\_p} = 0.0000076$, $\beta_{njm\_up} = 0.0003639$, $\beta_{jm} = 0.428571$.

Extracellular

$$v_{Xsub\_peak} \approx \left[\beta_{njm} R_{njseal} + \left(\beta_{jm} + n\beta_{njm}\right) R_{jseal}\right] C_m \cdot \frac{dv_{msub}(t)}{dt} + \beta_{jm} R_{jseal} C_m \cdot \frac{dv_{msub}(t)}{dt}$$
$$= [0.0003715 \times 900 + (0.428571 + 4 \times 0.0003715) \times 0.7] \times 23.3 \times 2 + 0.428571 \times 0.7 \times 23.3 \times 2 = 29.61 + 13.98 = 43.59\ \mu\text{V}$$

$$v_{XAP\_peak} = -\left[\beta_{njm} R_{njseal} + \left(\beta_{jm} + n\beta_{njm}\right) R_{jseal}\right] C_m \cdot \frac{dv_{mAP}(t)}{dt} - \beta_{jm} R_{jseal} C_m \cdot \frac{dv_{mAP}(t)}{dt} =$$
$$= -[0.0003715 \times 900 + (0.428571 + 4 \times 0.0003715) \times 0.7] \times 23.3 \times 7.5 - 0.428571 \times 0.7 \times 23.3 \times 7.5 = -111.03 - 52.42 = -163.45\ \mu\text{V}$$

Intracellular-like

$$v_{Xsub}(t) = \frac{nR_{jseal} + R_{njseal}}{nR_{jseal} + R_p + R_{njseal}} v'_{msub}(t) + \left[\beta_{njm\_up} R_{njseal} + \left(\beta_{jm} + n\beta_{njm\_up}\right) R_{jseal}\right] C_m \cdot \frac{dv'_{msub}(t)}{dt} + \beta_{jm} R_{jseal} C_m \cdot \frac{dv'_{msub}(t)}{dt}$$

Thus,

$$v_{Xsub\_peak} = \frac{nR_{jseal} + R_{njseal}}{nR_{jseal} + R_p + R_{njseal}} v'_{msub\_peak} = \frac{4 \times 0.7 + 900}{4 \times 0.7 + 2142 + 900} \times 10 \text{ mV} = 2.9651 \text{ mV}$$

$$v_{XAP}(t) \approx \frac{R_{njseal}}{R_p + R_{njseal}} v'_{mAP}(t) - \frac{R_p R_{jseal}}{R_p + R_{njseal}} C_{jm} \cdot \frac{dv'_{mAP}(t)}{dt} - \left[\beta_{njm_{up}} R_{njseal} + \left(\beta_{jm} + n\beta_{njm_{up}}\right) R_{jseal}\right] C_m \cdot \frac{dv'_{mAP}(t)}{dt} - \beta_{jm} R_{jseal} C_m \cdot \frac{dv'_{mAP}(t)}{dt}$$

Thus,

$$v_{XAP\_peak} \approx \frac{R_{njseal}}{R_p + R_{njseal}} v'_{mAP\_peak} = \frac{900}{2142 + 900} \times 75 \text{ mV} = 22.1893 \text{ mV}$$

3. Discussions

3.1 Nanoprotrusion-membrane interface as a perfect model to derive unique solutions

Generally, extracellularly recorded field potentials can be quite complicated to interpret, because of the unknown current sources from many potential neurons in the same volume conductor. Fortunately, this problem under current consideration is unique in that the nanoprotrusion-cell membrane interface as shown in Figure 1C is a well-isolated nano environment to study, which is minimally interfered by the macro cell-electrolyte environment often involving multiple adjacent cells in the same culture. It is reasonable to assume that the cell membrane involved in this nanoscale junctional interface can be excited uniformly, thus avoiding the hassle of spatial nonuniformity and greatly simplifying the problem for an intuitive analysis.

3.2 Thoughts on biophysics of the nanojunctional membrane after electro- or optoporation

During poration, the nanojunctional membrane gradually becomes permeable to all ion types, which migrate down their respective electrochemical gradients across the membrane, generating highly localized transient currents. Because the area of the nanojunctional membrane is very tiny, the electroporation process lasts at least a few seconds and the optoporation is usually completed in tens or hundreds of milliseconds, these local transient currents are minute; and because the inward $I_{Na}(j\omega)$ and outward $I_K(j\omega)$ flow simultaneously, their effects could cancel out with each other with minimal effects on the transmembrane voltage. Due to the diffusion constraint through the nanojunction to the cell-substrate junction and buck electrolyte, the ion distributions across the nanojunctional membrane may achieve new local equilibria, particularly with the concentrations of each ion type in the nanojunction equal to those in the cytosol. In this case, since no Na^+ and K^+concentration gradients exist across the nanojunctional membrane, AP cannot fire locally, not even to consider whether intact Na^+ and K^+ channels are still present there.

However, it is possible for the nanoprotrusion to distort the distributions of transmembrane ion channels, as well as changing the local membrane capacitance. These nonlinear distortions could cause the current densities across the nanojunctional membrane to deviate from those across an intact membrane, resulting in distortion to the waveforms and reduction to the amplitudes of $I_{Cnjm}(j\omega)$ and $I_{njm}(j\omega)$. Consequently, $V_X(j\omega)$ could be slightly distorted and attenuated.

3.3 Types of excitable cells

In many of these studies, cardiomyocytes and/or HL-1 cells were used for their large size and spontaneous rhythmic APs. It is noted that atrial cardiomyocytes and pacemaker HL-1 cells have

a slow inward depolarizing current $I_{Ca}(j\omega)$ in place of $I_{Na}(j\omega)$, whereas ventricular cardiomyocytes and non-pacemaker HL-1 cells have a slow inward $I'_{Ca}(j\omega)$ in the middle course of $I_K(j\omega)$, which creates a plateau phase during repolarization. As most of these studies employed pacemaker cells as a convenient spontaneous signal source, we can simply replace $I_{Na}(j\omega)$ with $I_{Ca}(j\omega)$ where appropriate when these cells were used, but will keep using $I_{Na}(j\omega)$ for generality.